ROUGHNESS AND WEAR RESISTANCE MODIFICATIONS INDUCED BY CYCLIC HIGH TEMPERATURE SHOCKS UPON A MICRO-COMPOSITE REFRACTORY ENAMEL

R.N. TURCU[1], I. PENCEA[2*], G. CHISIU[3], V. MANOLIU[4], M. BOTAN[5], M. BRÂNZEI[6], F. NICULESCU[7], A. C. POPESCU-ARGEȘ[8], M. IOAN[9], C.E. SFĂT[7]

A micro-composite enamel (MCRE_40) was developed to be a thermal barrier coating for aircraft engine parts made of EI868 superalloy. MCRE_40 underwent cyclic thermal shock tests (CTST). The paper addresses the roughness and micro-wear resistance induced by CTSTs. Autocorrelation and comparative frequency analyses were introduced to reveal the natures of the factors that induce the roughness. The correlation between roughness and the CTST parameters are two novelties addressed in the paper. The CTSTs increases the micro-abrasion wear resistance of MCRE_4,except one case. The experimental data about MCRE_40 which underwent CTSCs in 900-1150 °C are other novelty addressed in the paper.

Keywords: micro-composite refractory enamel, thermal barrier, cyclic thermal shock test, roughness, micro-abrasion wear resistance, autocorrelation

1. Introduction

Multifunctional coatings have become an emerging field over the last few decades in the aircraft industry, power plant, automotive etc. [1-5]. The multifunctional thermal barrier coatings (TBC) are used in aeronautics to protect the hot working parts of the turbojet engines [4-7]. Among TBCs, refractory

[1] PhD., Metallic Materials Science & Physical Metallurgy Department, University POLITEHNICA of Bucharest, Romania, e-mail: ramona.nicoleta.turcu@gmail.com;
[2] Prof., Metallic Materials Science & Physical Metallurgy Department, University POLITEHNICA of Bucharest, Romania, ini.pencea@gmail.com ;
[3] Lecturer, Faculty of Mechanical Engineering and Mechatronics, University POLITEHNICA of Bucharest, Romania, e-mail: georgiana_bosoi@yahoo.com
[4] Sci.Res. I, National Institute for Aerospace Research "Elie Carafoli", Bucharest, Romania, e-mail: vmanoliu@yahoo.com
[5] Sci. Res, National Institute for Aerospace Research "Elie Carafoli" – INCAS, Bucharest, Romania, e-mail: botan.mihail@incas.ro
[6] Assoc.Prof., Metallic Materials Science & Physical Metallurgy Department, University POLITEHNICA of Bucharest mihaibranzei@yahoo.com;
[7] Lect., Faculty of Materials Science and Engineering, University POLITEHNICA of Bucharest, Romania, e-mail: flori.pereteanu@yahoo.com;sfateugen@yahoo.com
[8,9] PhD Candidate, Faculty of Materials Science and Engineering, University POLITEHNICA of Bucharest, Romania, e-mail: arges_alina@yahoo.com; mihaita.ioan@gmail.com.

enamels stand out with the highest performance/cost ratio. The enamel can be considered as a thermodynamic system entrapped into a frozen equilibrium states at low temperature (300 -500 K). If the system is heated, then the system emerges from the frozen equilibrium state and is prone to complex processes [8-12]. Hence, thermal socks can significantly modify the phase composition of a TBC and implicitly its functional performances. To our present knowledge, this issue is not dealt with in the literature.

The paper addresses the modifications induced by cyclic thermal shock tests (CTST) into an enamel coating, especially its roughness, in conjunction with modifications in erosion resistance. For the exploration of these induced modifications, roughness, micro-wear abrasive measurements, optical microscopy (OM) and SEM-EDS observations were carried on the tested and witness samples. Also, paper presents SDAR-OES and ED-XRFS data regarding the compositions of the support and of the coating.

The roughness effect upon the erosion resistance was investigated by Calowear method [13]. This choice is another novelty of the paper as the micro-abrasion wear is the single one method compatible to the hot erosion which enamel underwent during service.

The paper introduced an innovative approach for identification of the random and/or systematic effects that induce the surface roughness. Thus, it was introduced the short range and long range autocorrelation analyses to reveal where or not there is a correlation along the roughness patter.

The paper presents the following important novelties:

- A holistic approach to characterizing the roughness of MCRE_40 email
- Original data about the effects of the CTST parameters on the roughness of MCRE_40 enamel.
- Original data about the effects of the CTST parameters on the micro-abrasion resistance of MCRE_40 enamel. Also, the data obtained are extremely useful for guiding future research aimed to produce an improved version of the MCRE_40 enamel.

2. Materials and methods

2.1. Materials

The researches were carried on MCRE_40 that coat pieces of EI_868 superalloy. The elemental composition of the substrate measured with a SpectromaxX SDAR-OES spectrometer is shown in Table 1. The measurements data are presented together with their expanded uncertainty having 95% confidence level, U(95%). The prescribed composition of EI_ 868 is given in the first row of Table 1[14].

Table 1.

Elemental composition of the substrate [%] mass

Element	**C**	**Si**	**Mn**	**Cr**	**Ni**	**Mo**	**Fe**	**W**	**Al**	**Ti**	**S**	**P**
EI_868 [14]	≤0,10	≤ 0.80	≤0.50	23,50-26,50	25.0-30.0	≤1.50	≤4.0	13.00-16.00	≤0.5	0.3-0.7	≤0.013	≤0.013
c	0.12	0.39	0.33	23.53	25.52	1.10	2.41	14.00	0.30	0.66	0.004	0.007
U(95%)	0,04	0,08	0,06	0,04	0,04	0,08	0,10	0,6	0,08	0,12	0,002	0,006

The comparative analysis of the data in Table 1 shows that the EI_868 alloy is not compliant regarding the concentration of C. However, if the expanded measurement uncertainties are considered, it can be stated that the substrate composition corresponds to the predicted mark.

In order to increase the refractoriness of the enamel, a frit recipe with moderate fondant content (B_2O_3) was adopted. Also, Al_2O_3 oxide was added for the same reason, as it is shown in Table 2.

Tabel 2.

The nominal composition of the frit (wt%)

SiO_2	BaO	Cr_2O_3	B_2O_3	Al_2O_3	CaO	MgO	ZnO	Mo_2O_3
40.0	30.0	10.0	3.0	3.0	4.0	2.5	4.5	3.0

The fine grained frit were mixed with powdered Cr2O3, water and surfactants to obtaine the slury called barbotine, whose oxide composition is presented in Table 3.

Table 3.

The composition of the barbotine (wt%)

Substance	Frit	C_2O_3	MT530 clay	Distilled water	NaO
[%] wt	100	30	10	50	10

Samples of_ EI 868 sheets (50x25x1.2 mm) were prepared by corundum blasting, alcohol degreasing and subsequently coated on a single side by wet spray process. The coated specimens were fired at 1350 ^{o}C for 3 min in an electrical furnace. The oxidic composition of the enamel coatings measured with Xepos XRF spectrometer is given in Table 4.

Table 4.

The oxidic commposition of the MCRE_40 enamel

SiO_2	BaO	Cr_2O_3	B_2O_3	Al_2O_3	CaO	MgO	ZnO	Mo_2O_3	NaO
27,6	20,7	27,6	2,3	2,1	2,8	1,7	3,1	2,1	10,0

The CTSTs were performed with a special equipment built at SC INCAS SA, which is described elsewhere [15]. A thermal shock test encompasses a sharp transition of the specimen from room temperature into a furnace chamber at higher temperature (900 ^{o}C-1150^{o}C), a 5 minutes exposure at this temperature followed by a transition from furnace into a cool air jet, which cool down the specimen at room temperature in 3 minutes. This process is repeated automatically for 200 cycles. The temperatures inside the furnace were: 900 ^oC, 1000 ^oC, 1050 ^oC, 1100 ^oC, 1150 ^oC. The coolant jet is provided by a tank containing air at 5 atm. The temperature profiles of the heating and cooling stages of the CTST are automatically monitored with an accuracy of ± 1 ^oC.

2.2. Methods

The measuring principle of the Calowear is well known and is described many papers [16-18]. An extended version of the Archard law was used for the estimation the micro-abrasion wear resistance of a coating-substrate system [17]:

$$N\left(\frac{96R}{\pi b^4}\right) = \left(\frac{1}{K_c} - \frac{1}{K_s}\right)\left(\frac{16Rt}{b^2} - \frac{96R^2t^2}{b^4}\right) + \frac{1}{K_s} \tag{1}$$

where SN is the slip distance multiplied by the applied load; R is the ball radius; b is the inner wear crater diameter; Kc is the wear coefficient of the coating and Ks of the substrate respectively, Vc and Vs are the measured wear volumes.

The wear resistance (WR) was estimated by K^{-1}, respectively:

$$WR = \frac{1}{K} = \frac{SN}{V} \tag{2}$$

In order to substantiate the influence of the thermal shock on the EI_868 enamel/superalloy system, SEM investigations and EDS analyzes of the enamel-substrate interface were performed. The QUANTA 200 microscope (SEM / ESEM-EDAX) was used for this purpose.

The surface roughness is quantified by a set of measurements Ra, Rz, Rq, Rv, Rp, Rsm, Rpc, Rpk, Rvk, Rsk, Rmax which are intended to reveal certain aspects associated with roughness [16, 19-22]. Among them, we used the followings:

$$R_a = \sqrt{\frac{\sum_{i=1}^{N} |y(i)|}{N}} \tag{3}$$

where N is the number of offset measurements; y(i) is the offset i.e. the distance between the measurement point and the reference line.

$$R_q = \sqrt{\frac{\sum_{i=1}^{N} y^2(i)}{N}} \tag{4}$$

Rz is the average of the absolute values of 5 highest peaks and 5 deepest valleys of the roughness patterns. Rz is a measure of the highest roughness of the surface. Skewness, Rsk, is a measure of the asymmetry of the profile about the mean line and it is calculated as:

$$R_{sk} = \sqrt[3]{\frac{\sum_{i=1}^{N} y^3(i)}{N}} \tag{4}$$

The paper introduces a new way of analyzing the surface texture using the autocorrelations, which is designed to highlights the random or systematic nature of the effects that induced roughness during CTSTs. Thus, the autocorrelation parameter AC(k) is calculated as:

$$AC(k) = \frac{\sum_{i=0}^{i=N-k} y(i)y(i+k)}{\sum_{i=0}^{i=N} y(i)^2} \quad (5)$$

where y(i) is the stylus offset from roughness reference level at the i^{th} step; k is the displacement of the cloned roughness profile related to the original one.

Another novelty introduced by the paper consists in an comparative analysis of the frequencies of the y(i) offset values to the frequencies calculated based on a normal distribution N (μ, σ) (Gauss-Laplace) whose parameters (μ, σ) are calculated based on the experimental data [23].

The roughness measurements were carried on with a INSIZE ISR-C002 instrument which automatically acquires the data. The evaluation length was 12.5 mm for all specimens, with a pitch of 4.4 µm, that means 2857 measurement points. In order to ensure a good statistic for the calculation of the roughness parameters, 5 measurements were carried out under repeatability conditions.

3. Results and discussions

The MCR_40 specimens that undergone CTST were denoted as follows: MCRE_40-0, untested; MCRE_40-1, tested at 900 ^oC; MCRE_40-2, tested at 1000 ^oC; MCRE_40-3 tested at 1050 ^oC; MCRE_40-4 tested at 1100 ^oC and MCRE40-5, tested at 1150 ^oC. The morphological aspects of the witness specimen and of the CTST ones are shown in Fig. 1.

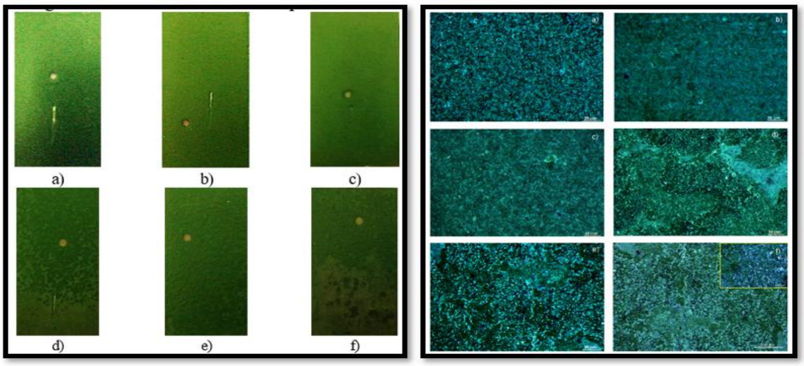

i ii

Fig. 1 Morphological images of the enamel surfaces: i) at lower magnificataion: a) MCRE_40_0; b) MCRE_40_1; c) MCRE_40_2; d) MCRE_40_3; e) MCRE_40_4; f) MCRE_40_5; ii) at higher magnification

The specimens tested at 900 ^oC and at 1000 ^oC does not show significant morphological modifications; also, the color of the enamel remains unchanged. The specimens tested at 1050 ^oC, 1100 ^oC and 1150 ^oC show superficial morphological changes and the enamel color acquires an increasingly darker shade of green. A micro-structural analysis supports the same above-mentioned features but reveal much better the roughness increasing as the temperature of the CTST increases (Fig. 1). The CTSTs cause much subtle modification inside the enamel with affect the surface morphology, but also to the level of interface, which is responsible for the enamel adherence to substrate, thermal stress damping etc. as is depicted in Fig. 2.

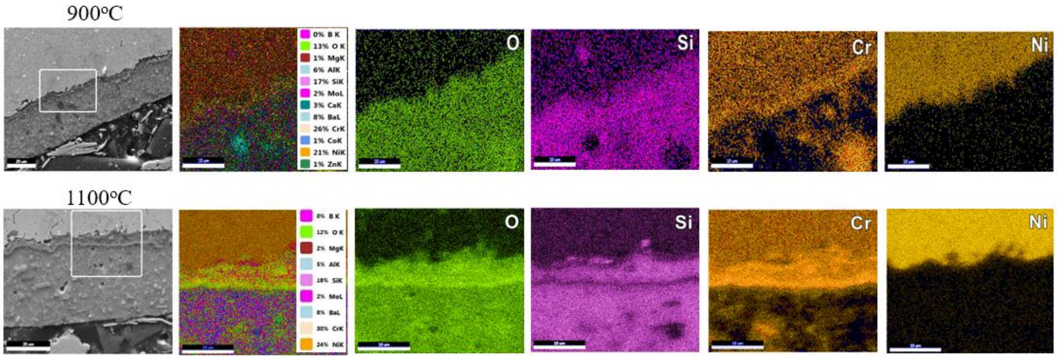

Fig. 2. Comparative SEM and EDS images of the specimen CTST at 900°C and at 1100°C

The CTST strongly promote the Cr selective diffusion at interface, given rise to a thin layer. The distributions of the Ni, Si, O major elements seems to be not affected by CTST as is shown in Fig. 2. The procedure for roughness measurement consists of acquiring 5 roughness patterns in repetitive conditions (Fig. 3.a) followed by data processing as to calculate the representative roughness parameters for each specimen.

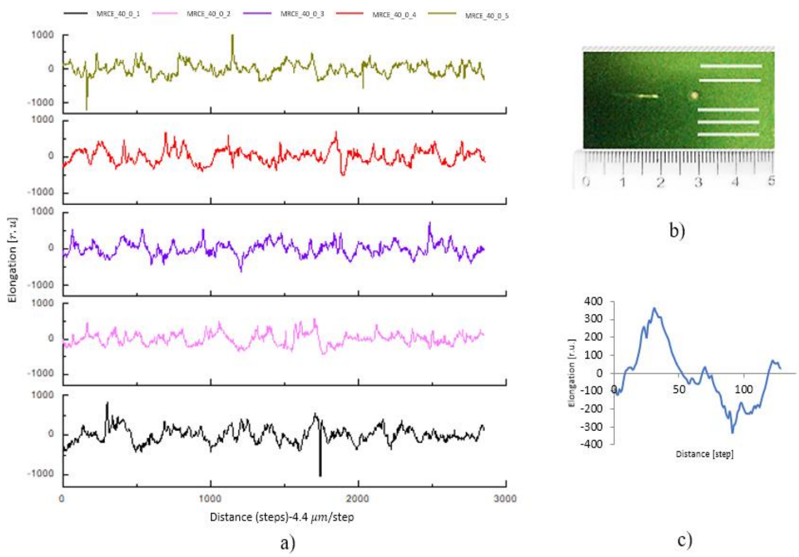

Fig. 3. a) Roughness profiles; b) locations of the roughness measurement; c) detail of a roughness pattern

The Ra, Rq, Rz and Rsk were considered the most representative roughness parameters (table 5)

Table 5.

Roughness parameters values calculated for the MCRE_40_0 specimen

	Pattern No.	**Ra** [μm]	**Rq** [μm]	**Rz** [μm]	**R**sk [μm]
MCRE_40_0	1	1.493	1.845	10.332	0.134
	2	1.331	4.594	10.254	0.133
	3	1.433	5.524	9.869	0.149
	4	1.579	1.894	9.499	0.215
	5	1.480	1.868	11.296	-0.170
Mean		**1.463**	**3.145**	**10.250**	**0.092**
Standard deviation		**0.091**	**1.778**	**0.673**	**0.150**

Fig. 4a) shows the histogram of the frequencies of the Ra obtained on sample MCRE_40_0 in the third run. In Fig. 4 b) are presented the graphs corresponding to the measured frequencies (blue line) and the simulated frequencies based on a normal distribution (Gauss- Laplace) with mean $\mu = -6$ μm and standard deviation $\sigma = 280$ μm. This simulation aims to reveal the nature of the factors that contribute to the roughness generation i.e. random or systematic.

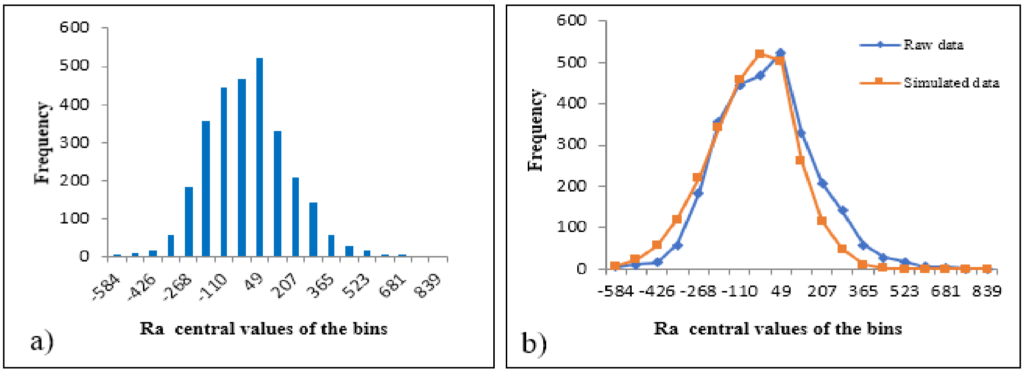

Fig. 4. a) Histogram of the absolute frequencies associated to the profile no. 3. b) comparative absolute frequency distributions

The frequency simulation with the Gaussian distribution (orange line) shows that the roughness has a normal behavior which attests the random nature of the factors that generates the roughness. Also, Fig. 4 shows the monomodal frequency distribution, which supports once again the random nature of the MCRE_40_0 roughness. The above simulation was performed for each profile in Table 5 and it was observed that the frequency distribution of the y(xi) values shows a strong monomodal clustering behavior.

The random or the systematic nature of the roughness is much better revealed by the autocorrelation analysis performed at short and long range displacement of the cloned profile. The small range autocorrelation analysis was performed with pattern displacement from 1 to 15 steps, while the long range one with pattern displacement from 20 to 180 steps. The autocorrelation analysis was applied to each pattern as it is shown in Fig. 5.a,b.

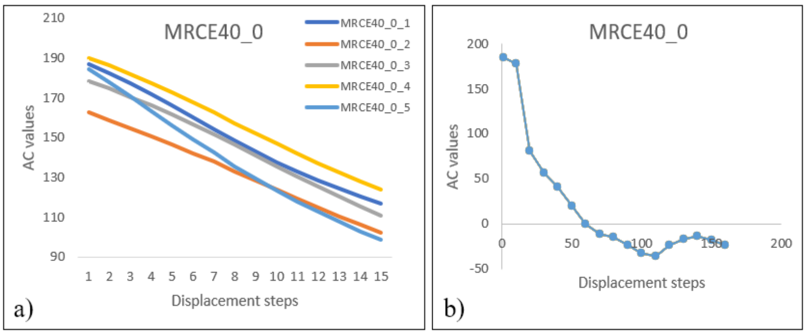

Fig. 5. The dependency of the AC values on the stepped displacement: a) short range autocorrelation; b) long range autocorrelation

Fig. 5 shows that the AC values decrease monotonically at shot range while at long range the value of AC decreases in the 20-100 range and, subsequently, it fluctuates, but takes smaller values. The AC graphs do not show periodicity. The periodicity missing clearly shows the random nature of the factors that determine the roughness of the specimen. The above procedure for roughness characterization of the MCRE_40_0 specimen was applied to all specimens that undergone CTST. The mean values of the Ra, Rq and Rz parameters assigned to the specimens MCRE_40_0-:- MCRE_40_5 are posted in Table 7. Data in Table 7 clearly shows that the roughness of the enamel coatings increases as the upper temperature of the CTST increases.

Table 7.

The mean values of the Ra, Rq and Rz parameters assigned to the specimens MCRE_40_0--MCRE_40_5

	Ra [µm]	Rq [µm]	Rz [µm]	Rsk
MRCE40_0	1.463	3.145	10.25	0.092
MRCE40_1	1.819	2.324	13.821	-0.251
MRCE40_2	1.815	2.284	12.655	-0.251
MRCE40_3	7.219	8.875	38.967	0.840
MRCE40_4	3.144	3.838	18.392	0.073
MRCE40_5	8.494	10.177	42.331	-0.750

The increasing of the roughness parameters (Table 7) when the upper temperature of the CTST increase is a negative finding, as a higher roughness detrimentally affect the functional characteristics of a coat. Also, the roughness profile changes its frequency distribution of y(i) as the upper temperature of the CTST increases (Fig. 6). The absolute frequency distribution of y(i) widens as the upper temperature of the CTST increases and tends to become bimodal, which indicate that enamel suffered severe damage by delamination and crunching.

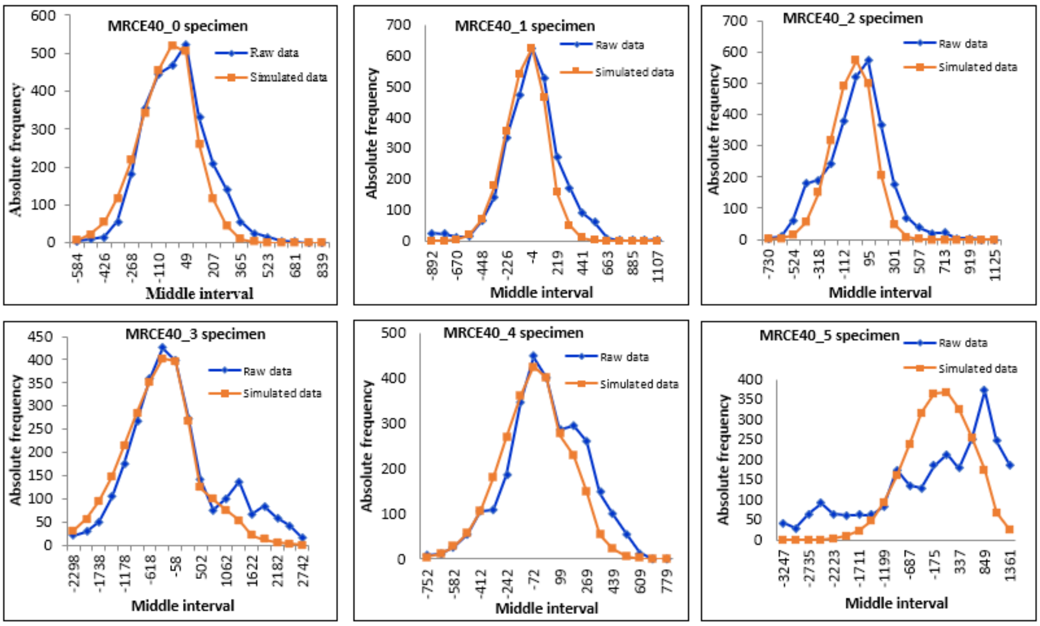

Fig 6. The raw and simulated frequency distributions assigned to the witness and to the CTST specimens

The missing of the AC periodicity and the monotonically decreasing of the AC values in the [0, 100] step range (Fig. 7) are the most relevant for the random nature of the factors that determine the roughness of the specimens.

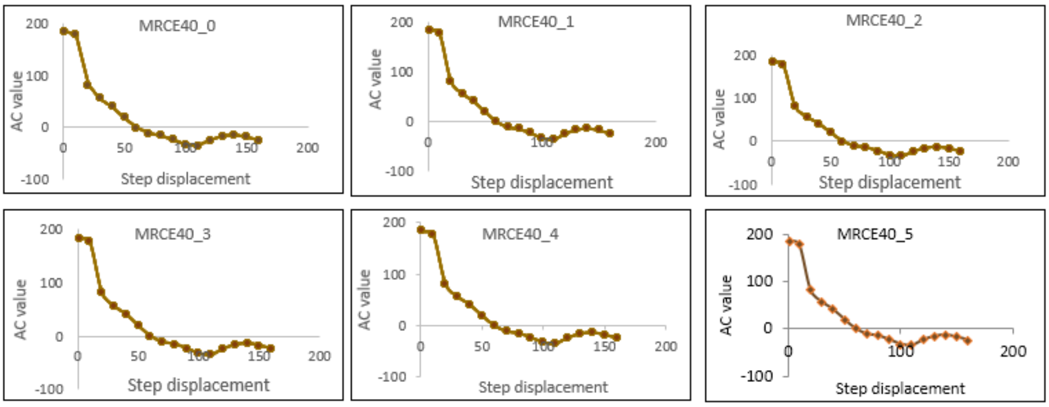

Fig. 7. Graphs of the long range autocorrelation of the roughness values assigned to the witness and to the CTST specimens

The micro-abrasive wear tests were carried out with a steel ball having a diameter of 24.5 mm, which provides a normal force of 0.57 N. Each test lasted

15 min. The contact between the ball and the specimen was wetted with a slurry made of 5 g of SiC particles, (4.5 µm in diameter) and 250 ml of distilled water. The tests have generated perforated wear craters for all coatings as it is shown in Fig. 8, except the MCRE_40_5 which was improper for this test as the enamel coating is about totally damaged by the undergone CTST.

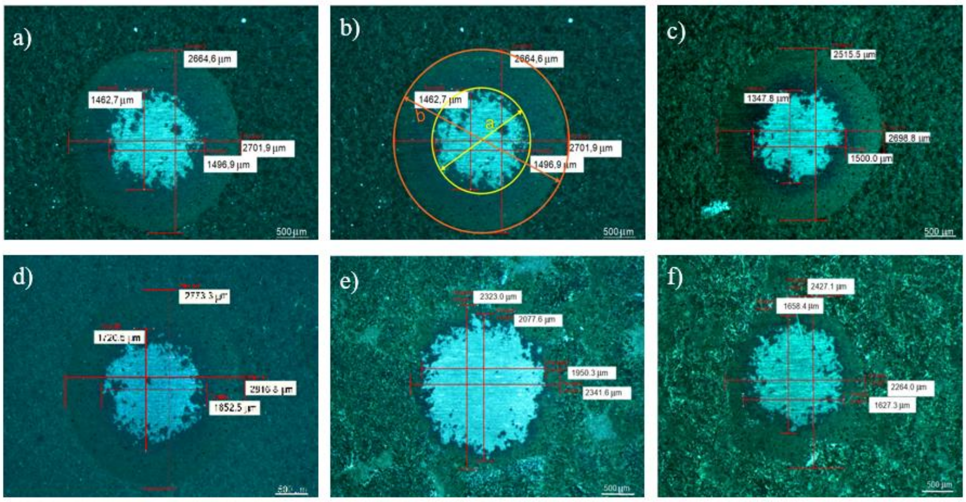

Fig. 8. Images of the wear craters into specimens: a) MRCE40_0; b) delimitation of the wear crater into MRCE40_0; c) MRCE40_1; d) MCRE40_2; e) MCRE40_3; f) MCRE40_4

The outcomes of the Calowear tests are given in Table 8 which shows a complex dependency of the WR of enamel (WR_E) on CTSTs temperatures.

Table 8

Results of micro-abrasive wear tests carried on

Specimen	b [mm]	a [mm]	t [µm]	V_E [mm3]	K_E [m^3/J] *10^6	V_S [mm^3]	K_S [m3/J] * 10^6	WR_E [J/mm^3]	WR_S [J/mm^3]
MRCE40_0	2.7	1.5	51.4	0.19	1596	0.0203	168	627	5951
MRCE40_1	2.6	1.4	49.0	0.17	1389	0.0154	128	720	7842
MRCE40_2	2.8	1.7	50.5	0.21	2094	0.0335	329	478	3037
MRCE40_3	2.3	2.0	13.2	0.05	472	0.0641	631	2117	1586
MRCE40_4	2.3	1.6	27.9	0.09	676	0.0262	207	1480	4839

4. Conclusions

The micro-composite MCRE_40 enamel can be considered a thermodynamic system entrapped in a frozen equilibrium states at room temperature. When the enamel is heated then the system leaves the frozen equilibrium state and it is prone to a complex process: solid state phase transformations, crystallization, segregation, oxidation of the substrate, etc.

The OM, SEM and EDS observations clearly demonstrate that the enamel morphology and structure are modified due to CTSTs. These modifications imply modification of the functional performances. As the upper temperature of the CTST increases, as the roughness parameters of the MCRE40 increase, which is a shortcoming of MCRE40. The enamel roughness induced by CTSTs show random patterns as were revealed by the frequency distribution comparative analyses and by the autocorrelation studies.

WR_E of the MCRE40 does not show a monotonically dependence on the upper temperature of the CTST. Further supplementary experimental are needed to clarify such a complex behavior. The findings addressed in the paper indicate the need of further researches for improving the resistance of the enamel to roughing and to hot erosion under dynamic hot working conditions.

R E F E R E N C E S

1. *S. M. Lakiza, M. I. Grechanyuk, O. K. Ruban, V. P. Redko, M. S. Glabay, O. B. Myloserdov, O. V. Dudnik, S. V. Prokhorenko,* "Thermal Barrier Coatings: Current Status, Search, and Analysis", Powder Metallurgy and Metal Ceramics, **2018,** Vol. **57**, Nos. **1-2**, May, (Russian Original Vol. 57, Nos. 1-2, Jan.-Feb., 2018)
2. *A. Lepeshkin*, Investigations of Thermal Barrier Coatings for Turbine Parts *Russia*, Ceramic Coatings, chapter Investigations of Thermal Barrier Coatings for Turbine Parts, in volume – Applications in Engineering, www.intechopen.com(*Central Institute of Aviation Motors*), **2017**
3. *Marius Panţuru, Vlad Cârlescu, Daniela Chicet, Lucia Răileanu, Corneliu Munteanu*, Evaluation of Adhesion – Cohesion of Some TBCs Used for Internal Combustion Engine Valves Using Scratch Method, U.P.B. Sci. Bull., Series B, **2019,** Vol. **81**, Iss. **2**, ISSN 1454-2331.
4. *B. Gleeson*, Thermal barrier coatings for aeroengine applications. Journal of Propulsion and Power, **2006. 22(2): p. 375-383**.
5. *M. Wu, M. Chen, S. Zhu, F. Wang,* Protection mechanism of enamel–alumina composite coatings on a Cr-rich nickel-based superalloy against high-temperature oxidation, in Surf Coat Technol. **2016**; **285**, p. 57–67.
6. *A. Zucchelli , G. Palombarini, F. Tarterini, L. Pignatti, A. Pirazzoli, Viale del Risorgimento, S. Felice*, Self-healing concept to improve the mechanical performance of vitreous enamel coated steel, 2007, Proceedings of the First International Conference on Self Healing Materials 18-20 April **2007**, Noordwijk aan Zee, The Netherlands
7. *C. Dumitrescu, I. Pencea, V. Manoliu, F. Vasiliu, F. Barca, R. Păunescu*, SEM, EDS and WAXD characterisation of a new enamel used as protective and thermal barrier coatings in aircraft engines, Conference Proceedings „The Coatings in Manufacturing Engineering", 14-15 October **1999**, Thessaloniki, Greece, p. 303-312
8. *M. Chen, M. Shen , X. Wang, S. Zhu, F. Wang,* Interfacial reaction between SiO2–Al2O3–ZnO–CaO based glass coatings and K38G superalloy substrates. Surf Coat Technol. **2013**; 216:145–151.

9. *Chen M, Zhu S, Wang F.* Crystallization Behaviour of SiO2–Al2O3–ZnO–CaO Glass System at 1123–1273 K. J Am Ceram Soc. **2010**; 93(10):3230–3235.
10. *M. Wu, M. Chen, S. Zhu, F. Wang*, Protection mechanism of enamel–alumina composite coatings on a Cr-rich nickel-based superalloy against high-temperature oxidation, in Surf Coat Technol. **2016**; 285, p. 57–67.
11. *I.G. Berdzenishvili*, Protective Glass Coatings for Chemical Equipment, Pipes and Pipelines, Georgian Technical University, Tbilisi, **2008**.
12. *M.Branzei, I. Pencea, A. A. Matei, C.E. Sfat, I. V. Antoniac, R. N. Turcu, V. Manoliu,* Influence of high temperature exposure on the adhesion of a micro-composite refractory enamel to a Ni-18-Cr-12W superalloy, J. of Adhesion Science & Technology, **2017**
13. *A M Petrescu, A. Tudor, G. Chisiu, N. A. Stoica, U Cihak Bayr*, "The determination of the thickness of the layers deposited on the electronic circuit boards through tribological methods", in IOP Conf. Ser.: Mater. Sci. Eng. vol.174, February **2017**. 012026
14. ** https://www.evek.biz/materials/splav-hn60vt-ei868-vg98.html, accessed on 12.11.2019, 19.36 h
15. *Victor Manoliu, Gheorghe Ionescu, Adriana Stefan,Constantin Serghie, Sorina Ilina, Constantin Vilcu*, Incas Quick Thermal Test Shock Installation - Qts1, Incas Bulletin No. 2/ **2009**
16. *R. Bethke, K. Schiffmann*, Ball Cratering Wear Test: Review of the State of the Art, Fraunhofer Institut fur Schicht und Oberflachentechnik, Braunschweig, May **2001**
17. *K. L. Rutherford, I. .M Hutchings,* A micro-abrasive wear test, with particular application to coated systems. Surface & Coatings Technology, 79 (**1996**) 231-239.
18. ***,https://www.predev.com/pdffiles/surface_roughness_terminology_and_parameters.pdf, accessed on 0.202013.45h
19. ***SR EN ISO 4287: 2003 Geometrical Product Specifications (GPS) - Surface texture: Profile method - Terms, definitions and surface texture parameters
20. *D. MacKenzie*, Surface Texture Measurement Fundamentals Willrich Precision Instrument
Co
Ph: 866-945-5742
 23,07,**2019**, https://willrich.com/wp-content/uploads/2014/11/Surface-Texture-Measurement-Fundamentals.pdf
21. *B. Muralikrishnan, J. Raja*. Computational Surface and Roughness Metrology. ISBN 978-1-84800-296-8, Springer, London **2009**, p.10-50
22. *J. Raja, B. Muralikrishnan, Shengyu Fu*. Recent advances in separation of roughness, waviness and form. Precision Engineering. Journal of the International Societies for Precision Engineering and Nanotechnology. 26 **(2002**), pp 222–235
23. *I. Pencea,* Metallurgy - Advances in Materials and Processes, Edited by Yogiraj Pardhi, Chapter 6 , "Multiconvolutional Approach to Treat the Main Probability Distribution Functions Used to Assess the Uncertainties of Metallurgical Tests ISBN 978-953-51-0736-1, 186 pages, Publisher: InTech, Chapters published September 19, **2012** under CC BY 3.0 license, DOI: 10.5772/2852